JOURNAL OF CRITICAL REVIEWS

ISSN- 2394-5125 VOL 7, ISSUE 15, 2020

ACCURATE PREDICTION AND ANALYSIS RESISTANCE COMPONENTS OF WOODEN FISHING BOATS USING OPENFOAM

Dr. Toan Le Van

Naval Architecture Department, Ho Chi Minh City University of Transport, VietNam

Received: 14 March 2020 Revised and Accepted: 8 July 2020

ABSTRACT: This paper presents the application of our published approach to accurately predict and analyze the total resistance along with its components for small and low-speed boats. In this study, ship resistance is computed using CFD (Computational Fluid Dynamics) method by the CFD open-source software OpenFOAM, where the viscous flow with the free surface around the ship hulls is simulated by the RANSE (Reynolds Averaged Navier Stokes equations), combined with a turbulence model SST k-ω (Shear Stress Transport), and solved by the VOF (Volume of Fluid) method, with PIMPLE algorithm implemented in the OpenFOAM solver. Case studies are two typical wooden fishing boats, denoted M1317A and M1319, which represent Vietnamese traditional wooden fishing boat fleet and have been tested in towing tank.

The contribution of this study is the result of determining the appropriate values of the CFD input parameters, including the computational domain size and the parameters of the SST k-ω turbulence model for small and low-speed wooden fishing boats like Vietnamese fishing boats. With these input parameter values, the deviations between the CFD-based total resistance and the corresponding testing data of the computational hulls at different speeds are less than 3%. From this research result, the essential features of the flow field around the hulls, the total resistance, and its components of the computational boat types will be analyzed and presented. These research results are necessary to optimize the wooden fishing boat hulls.

KEYWORDS: Resistance, CFD, OpenFoam, PIMPLE algorithm, SST k-ω turbulence model, Vietnamese fishing boat.

I. INTRODUCTION

Resistance prediction is one of the most important problems and is the basis to resolve many contents in the ship design such as choosing the engine power to match the hull, optimizing the hull form, designing of ship appendages like propellers, rudders or energy-saving devices, etc. There are currently also some methods but continuously increasing computational power leads to the use of the Computational Fluid Dynamics (CFD) method as an effective tool in the prediction of the ship hydrodynamic performance in general and resistance in particular [1], [2]. The studies presented in the Gothenburg 2010 workshop showed that the CFD method can achieve good results in ship hydrodynamic computation compared with the testing results [3]. Two recent reviews [4], [5] have also shown that the CFD approach can be a complementary tool to towing tank tests in ship design.

However, in one of our studies [6], we have shown that the CFD-based computational results will be dependent greatly on the input parameters values of the CFD solver which include the computational domain size and the turbulence model parameters used in the simulation process, And this has resulted in CFD-based ship resistance results are not always accurate and reliable. Therefore also in this study, we presented an approach to improve the accuracy of CFD-based resistance value by determining the appropriate values of input parameters for specific ship types This explains why there have been many studies using CFD to predict ship hydrodynamic in general and resistance in particular, but most are performed according to available computation steps and usually applied to standardized large or high-speed vessels [7], [8], [9], [10], etc.

Few studies show how to improve the accuracy of the CFD-based results and applied on small and low speed vessels like wooden fishing boats in Vietnam and some other countries in Asia. Hence in this paper, we present the application of our new approach to accurately predict the resistance of Vietnamese wooden fishing boat types using OpenFOAM which is the famous CFD open source software. Also from this research result, the essential features of the total resistance and its components will be analyzed to contribute to the theoretical basis to solve the optimization problem of wooden fishing hulls

ISSN- 2394-5125 VOL 7, ISSUE 15, 2020

II. MATERIAL AND METHOD

A) Ship resistance

The total ship resistance R_T in this study is determined as follows [2]:

$$R_T = R_P + R_F \quad (1)$$

where R_P is the pressure resistance, in this case, is a normal force to hull surface and it can be called the residual resistance or wave-making resistance as a ship moving in calm water; R_V is the viscous resistance that is the tangential force acting on the hull in the longitudinal direction.

We can also write an equation for total resistance in terms of dimensionless coefficients [2]:

$$C_T = C_P + C_F \quad (2)$$

where C_T, C_P, and C_F are the total resistance, wave-making resistance, and frictional resistance coefficients, which can be determined according to the known formulas shown in the specialized documents as follows:

$$C_T = \frac{R_T}{0{,}5\rho SU^2}; C_P = \frac{R_P}{0{,}5\rho SU^2}; C_V \ \frac{R_V}{0{,}5\rho SU^2} \quad (3)$$

where ρ is the water density ($kG.s^2/m^4$); S is the wetted surface area of the ship hull (m^2) and U is ship speed (m/s).

B) Numerical Approach and the OpenFOAM solver

Theoretically, there are some different approaches to predict ship resistance using CFD method but in this study, it is computed using OpenFOAM, an open source CFD software, in which the viscous flow with the free surface around the hull is simulated by Reynolds Averaged Navier Stokes Equations (RANSE) combined with turbulence model SST k-ω (Shear Stress Transport), The approach according to RANSE is currently considered the most effective for solving the complex viscous flows so it has been detailed in many relevant specialized documents [1], [12]. However, the application of the RANSE solution to predict the ship hydrodynamic in general, and the resistance in particular, using OpenFOAM software is rarely presented in detail [13]. Therefore, in this section, the use of Volume of Fluid (VOF) method with the PIMPLE algorithm included in OpenFOAM solver to obtain RANSE solution for resistance prediction is presented instead of the basic theory of CFD method with RANSE which can be found in other references.
Although there are also currently many commercial CFD solvers, OpenFOAM, which is a CFD free open source software as a collection of libraries, has been widely used to numerically simulate and solve efficiently the complex turbulent viscous flow around the ship hulls with and without free surface effect [14].

Consequently, continuity and momentum equations can be described as an incompressible Newtonian fluid in tensor form, as follows [1], [15]:

$$\nabla \bar{u} = 0 \quad (4)$$

$$\rho \frac{\partial \bar{u}}{\partial t} + \rho(\bar{u} \nabla)\bar{u} = \rho g - \nabla \bar{p} + \mu \nabla^2 \bar{u} + \nabla \bar{\sigma}_t \quad (5)$$

where $\bar{u}$, $\bar{p}$ present, respectively, the average velocity and pressure fields; ρ, μ is the fluid density and dynamic viscosity; g is the gravity acceleration; $\bar{\sigma}_t$ is the Reynolds stresses tensor, written in Einstein notation $\bar{\sigma}_t = -\rho \overline{u_i' u_j'}$ and can be modeled by the Boussinesq hypothesis for an incompressible flow which is computed by two equations of SST k-ω turbulence model [16].

ISSN- 2394-5125 VOL 7, ISSUE 15, 2020

$$-\rho\overline{u_i' u_j'} = \mu_t\left(\frac{\partial \bar{u}_i}{\partial \bar{x}_j} + \frac{\partial \bar{u}_j}{\partial \bar{x}_i}\right) - \frac{2}{3}\rho k\delta_{ij} \quad (6)$$

where μ_t is turbulent (eddies) viscosity, k is the turbulent kinetic energy, δ_{ij} is the Kronecker delta function, equals to 1 if i = j and 0 if $i \neq j$, u_i', u_j', $\bar{u}_i$, $\bar{u}_j$ are the fluctuating and mean velocity components, respectively [17].

SST k-ω is a hybrid turbulence model combined two standard turbulence models k-ω and k-ε to take advantage of both, with a k-ω model is used to simulate flow in the viscous sub-layer near the wall, k-ε model is used to predict the behavior of flow in regions away from the wall [18]. As a result, this model is effectively used throughout the flow field, including in the viscous sub-layer located near the wall, so it can also be used as a Low-Re turbulence model, which is appropriate for the small and low-speed vessels without any additional damping functions [19]. For computational fishing boats, their Reynolds number is around 4.658E+06 as moving at the design speed in calm water [6], so it can be classified as the Low-Re turbulent flow regimes. Another advantage of this turbulence model is the ability to take into account the transport of the principal turbulent shear stress in the adverse pressure gradient at the boundary layers. Therefore, it is reasonable that the SST k-ω model is best suited to realize a numerical prediction ship resistance, due to the high curvature of the wetted hull surface, the flow through the hull produces a high adverse pressure gradient at the boundary layers. The SST k-ω turbulence model in OpenFOAM Solver is governed by the following formulas [20]:

$$\frac{\partial k}{\partial t} + \frac{\partial (u_i k)}{\partial x_i} = \frac{\partial}{\partial x_i}\left[\left(\nu + \frac{\nu_t}{\sigma_k}\right)\frac{\partial k}{\partial x_i}\right] + P_k - \beta^* k\omega \quad (7)$$

$$\frac{\partial \omega}{\partial t} + \frac{\partial (u_i \omega)}{\partial x_i} = \frac{\partial}{\partial x_i}\left[\left(\nu + \frac{\nu_t}{\sigma_\omega}\right)\frac{\partial \omega}{\partial x_i}\right] + \alpha\frac{P_k}{\nu_t} - \beta\omega^2 + 2(1-F_1)\sigma_{\omega 2} - \frac{1}{\omega}\frac{\partial k}{\partial x_i}\frac{\partial \omega}{\partial x_i} \quad (8)$$

Closure coefficients and auxiliary relations:

$$F_1 = \tanh\left\{\min\left[\max\left(\frac{2\sqrt{k}}{\beta^*\omega y}, \frac{500\nu}{y^2\omega}\right), \frac{4\rho\sigma_{\omega 2} k}{CD_{k\omega} y^2}\right]^4\right\}; \quad F_2 = \tanh\left[\max\left(\frac{2\sqrt{k}}{\beta^*\omega y}, \frac{500\nu}{y^2\omega}\right)^2\right]$$

$$P_k = \min(P_k, \beta^* \rho k\omega); \quad CD_{k\omega} = \max\left(2\rho\sigma_{\omega 2}\frac{1}{\omega}\frac{\partial k}{\partial x_i}\frac{\partial \omega}{\partial x_i}, 10^{-10}\right); \quad \phi = \phi_1 F_1 + \phi_2(1 - F_1)$$

Table 1 shows the values of the above model constants [18].

Table 1. Model constants

β^*	α_1	β_1	σ_{k1}	$\sigma_{\omega 1}$	α_2	β_2	σ_{k2}	$\sigma_{\omega 2}$
0,09	5/9	3/40	0,85	0,50	0,44	0,0828	1,00	0,856

The presence of the free surface poses further problems for the solution of Eq. 9 outlined below. Among the techniques for computing two-phase flows, the interface capturing approach based on the Volume of Fluid (VOF) method is one of the most popular methods to solve the complex flows with the free surface [21]. The volume of fluid approaches treats the free surface as the solution of the advection of the fluid volume fraction α (ranging from 0 to 1) for each cell [22]. In this study, the volume fraction equation for density and viscosity are written as follows [23]:

$$\rho = \alpha\rho_{water} + (1 - \alpha)\rho_{air} \quad (9)$$

$$\mu = \alpha\mu_{water} + (1 - \alpha)\mu_{air} \quad (10)$$

The differential equation that governs the evolution of the scalar function α can be written as follows:

ISSN- 2394-5125 VOL 7, ISSUE 15, 2020

$$\frac{\partial \alpha}{\partial t} + \nabla(\alpha \bar{u}) = 0 \tag{11}$$

The discontinuity of the function α at the interface, represented by the jump, from 1 to 0, of the scalar quantity itself, commonly requires some special treatment in order to limit the numerical smearing and to predict the sharpest possible free surface shape [23]. The use of OpenFOAM libraries lets also to adopt a custom quasi-steady approach (*LTSInterFoam* library) to solve the time evolution of the free surface, and a quasi-steady approach is useful for each time step [13]. Attention only focuses on the steady-state solution which reached the end of a non-influent transient computation, and for this reason, the complex physic regulates the phenomenon [23]. In order to reach the steady-state condition as fast as possible, all the transient behavior of the solution can be partially neglected (violating, therefore, of the basic conservation equations) [5]. The *LTSInterFoam* solver is based on a Local Time Stepping approach (bounded, first-order accurate, implicit scheme) with time step is manipulated for each cell in the mesh, making it as high as possible according to the local Courant number to force the simulation to quickly reach steady-state. A smooth of the unphysical variation of the time steps across the whole domain cells is applied to prevent the instabilities caused by the sudden change in the time scale [14]. The selection Courant number is described in Eq.12:

$$C_R = U\frac{dt}{dx} \leq 1 \tag{12}$$

where dt is the time step; dx is the spatial step.

RANSE equations are numerically solved by using bounded second-order upwind schemes for all the spatial derivatives. Gradients are computed using second-order Gaussian integration, while Laplacian terms are treated with a conservative, unbounded second-order approach [12]. For the viscous flow with a free surface, there are two different approaches to capture the profile of the wave on the free surface: interface tracking method and interface capturing method [22]. The Volume of Fluid (VOF) method and the level-set method to capture the interface of the wave profile have been widely used for the complex flows due to its accuracy and efficiency. The VOF method uses a fixed mesh technique designed for multi-phase flows with the unknown interface position between the fluid flows which is found through the solution procedure [21]. In this study, the VOF method was implemented in the OpenFOAM solver to capture the free surface deformation, the PIMPLE algorithm was utilized to compute the pressure and velocity field as well as turbulent properties of the flow.

III. RESULT AND DISCUSSION

A. Ship geometry modeling

According to statistics in 2019, Vietnam had about 120,000 fishing boats and most of them are made of wood and built according to the traditional patterns and local fishermen's experience, without designing as well as computing the resistance. Generally, these boats have a small length (less than 25m), short parallel middle body length (about 10% of length overall of the ship) [24]. Two boat patterns, denoted M1317A and M1319, temporarily called study boats in this study, which represent Vietnamese typical traditional wooden fishing boats and have been tested in the model towing tank to obtain the resistance values at different speeds, are used for the calculation. Their lines and 3D hull forms which are modeled in AutoShip – a ship design software are illustrated in Figure 1 [6].

ISSN- 2394-5125 VOL 7, ISSUE 15, 2020

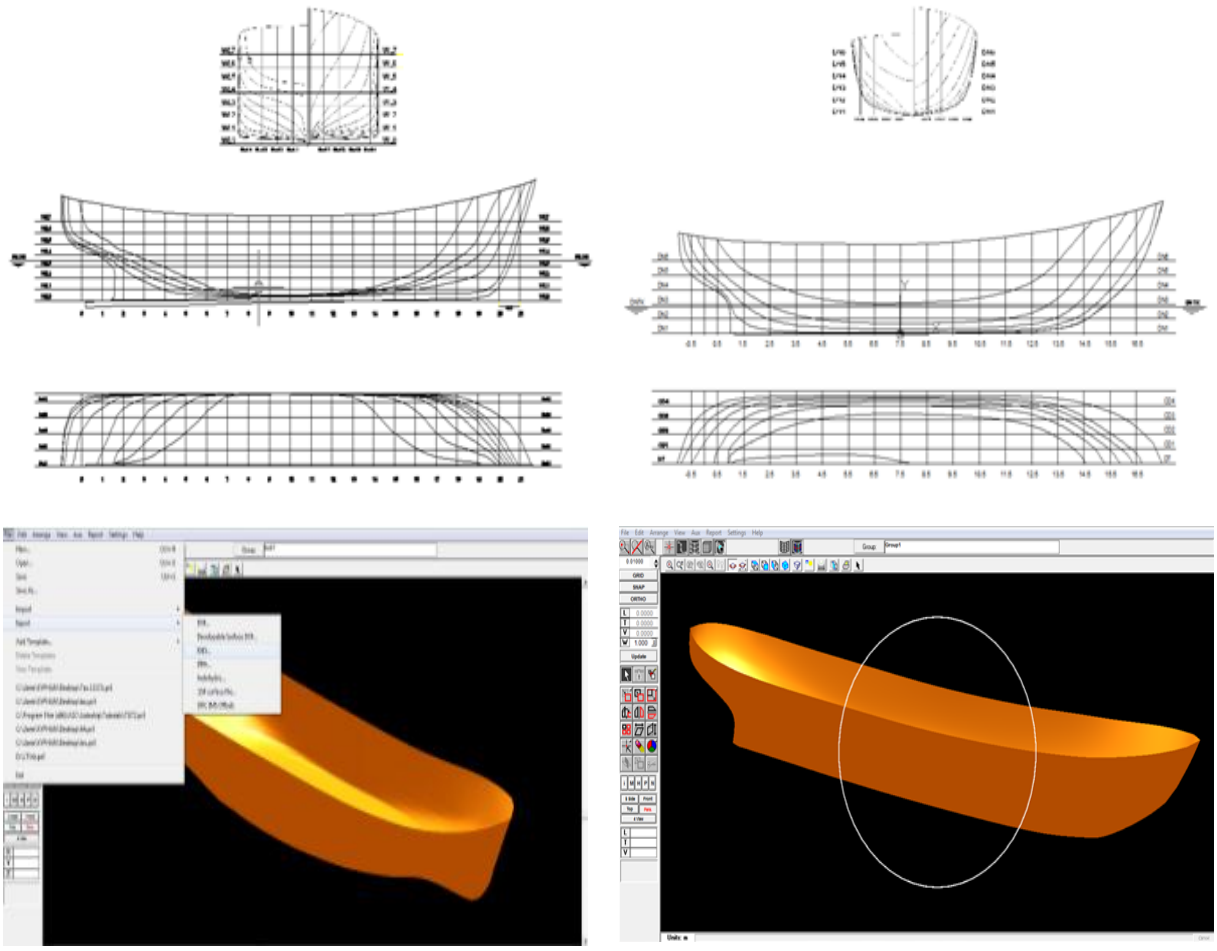

(a) M1317A hull (b) M1319 hull

Figure 1. The lines and 3D hull form of two study fishing boats

Table 2 presents the principal parameters of two study fishing boats in the full and model scale. The scale factor of the model used in the towing tank and the computational simulation is taken the same and equal to 1/7 [6].

Table 2. Main parameters of two study fishing boats

Ship parameters	Notation	Unit	M1317A boat		M1319 boat	
			Full scale	Model (1:7)	Full scale	Model (1:7)
Length overall	L_{OA}	m	21,900	3,129	17,400	2,485
Length of waterline	L_{WL}	m	18,550	2,650	14,287	2,041
Length between perpendiculars	L_{pp}	m	19,000	2,714	14,800	2,114
Maximum Breadth	B_{max}	m	4,480	0,640	3,880	0,554
Breadth of waterline	B_{WL}	m	4,480	0,640	3,140	0,448
Depth	D	m	1,900	0,271	1,500	0,214
Draft	d	m	1,225	0,175	0,735	0,105
Wetted areas	S	m^2	95,060	1,940	45,080	0,920
Midship coefficient	C_M	-	0,870	0,870	0,860	0,860
Block Coefficient	C_B	-	0,589	0,589	0,550	0,550
Prismatic Coefficient	C_P	-	0,677	0,677	0,639	0,639

ISSN- 2394-5125 VOL 7, ISSUE 15, 2020

Volume	□	m^3	61,170	0,178	19,51	0,057
Design speed	U_s	knots	8,645	3,264	9,125	3,445
Froude number	Fn	-	0,329	0,329	0,396	0,396

B. Mesh generation

The next computational step is to generate a discrete that accurately captures the hull surface. The quality of the mesh generation effects greatly on the reliability of the resistance prediction, therefore, the mesh should be fine with high-quality (well-shaped) cells, but without so many cells to make subsequent calculations intractable and match the hull surface as much as possible. In this study, SnappyHexMesh tool in OpenFoam is used to generate all computational meshes. This tool is a Cartesian hex-dominant mesh generation utility that can handle quite accurately complex geometries (starting from STL format representation of the geometric surfaces) with the capability to generate the prism layers, handle the curves, and perform the local refinements [20]. Figure 2 shows the mesh points on the current hull surface, and mesh distribution at the free surface and computational domain, in which to capture deformation of the free surface, and the speed of the flow near the wall, i.e the hull surface, the first fluid layer closest to the wall needs to be handle because the thickness of this layer significantly affects on the accuracy of the CFD solution when using the turbulence model. In this study, the thickness of this first fluid layer is estimated by the following formula [17]:

$$y = \frac{y^+ \mu}{\rho \sqrt{\frac{\tau_w}{\rho}}} \tag{13}$$

where τ_w is the shear stress on hull surface elements; ρ and μ is the density and dynamics viscosity of water, respectively.

Figure 2 also shows two local regions generated and refined, including 15 layers in the water-air intersection and 10 prism layers in the boundary layer around the hull with the absolute thickness of the first cell layer y = 0,013 m corresponding to y^+ approximate 300 for all computed cases. The mesh consists of about 1,3 million cells, with a maximum non-orthogonality of 75 and skewness below 3,5 [6].

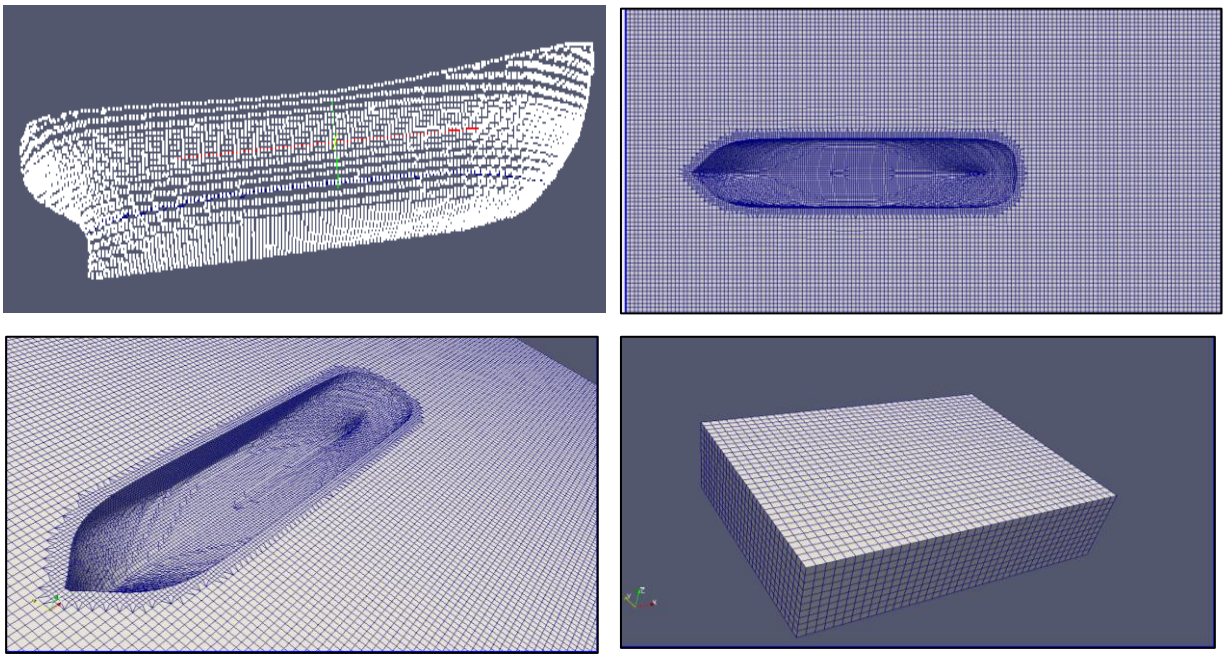

Figure 2. Surface mesh point and global mesh distribution

To prepare the input geometrical data file for OpenFOAM, the ship hull must be generated under STL (standard stereolithographic) format which is a triangulated representation of a 3D model. Figure 3 shows the code to

ISSN- 2394-5125 VOL 7, ISSUE 15, 2020

generate a discrete triangulation and a 3D model of computational hull surface was generated under the STL file format using OpenFOAM [6].

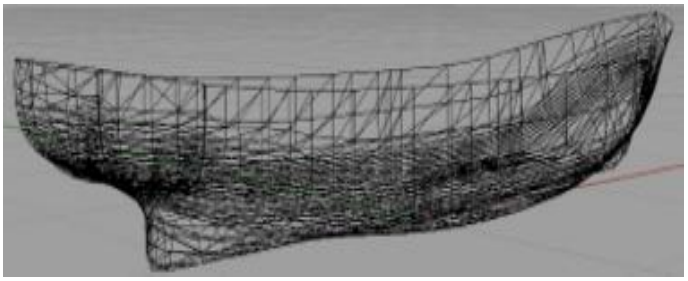

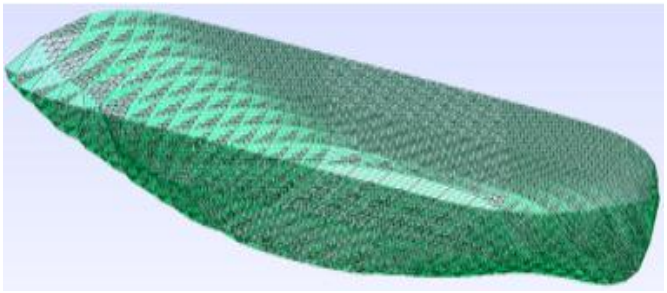

```
Vertices
(
    (x1 y1 z1)      // point 0
    (x2 y2 z2)      // point 1
      ……            // …
    (xn yn zn)      // point n
)
```

Figure 3. 3D hull surface under the STL file format and corresponding code

C. Determining the input parameters of CFD solution

In this study, the input parameters of CFD solution included computational domain size along with the position and value of boundary conditions and value of the turbulence model parameters. These parameters greatly affect CFD-based ship resistance but their values are generally not available to apply to specific ship types, and their appropriate values are also rarely published. Using the approach detailed in our published paper [25], in this section, the input parameter values suitable for two study boats will be determined by changing the value of the input parameters, in turn, to set up different case studies, also known as computational variations, then computing the hull resistance for each computational variation using the CFD tools and comparing with corresponding testing data to choose a most suitable variation where the deviation between the compared resistance values is stable and minimal.

1. Computational domain size and the boundary condition

Computational domain refers to a rectangular box space that is limited by boundary conditions around the ship hull to perform the numerical simulation process in the ship resistance prediction. In general, the boundaries used in CFD method are located at the boundaries of the computational domain including the inlet, outlet, side, bottom, wall, and symmetry plane as shown in Figure 4.

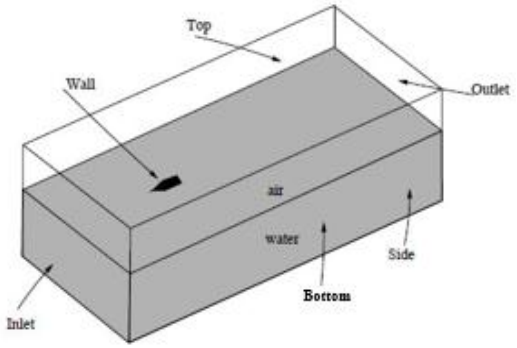

Figure 4. Size and position of boundary conditions of the computational domain

In this study, the boundary conditions which are used to predict resistance are chosen as follows: a uniform speed is specified at the inlet for both air and water phases, the zero gradient condition is set at the outlet, the hydrostatic pressure of air and water are be specified at the outlet domain. Due to the hull form is symmetrical so a symmetric condition is set on the symmetry plane and only half-flow around the hull is computed. The

ISSN- 2394-5125 VOL 7, ISSUE 15, 2020

side, top, and bottom boundaries are relatively far from the hull and they are set as rigid-slip walls. Finally, a no-slip condition wall is applied on the hull surface. The setting of the specific boundary condition is illustrated in Table 3.

Table 3. Boundary condition setting

Boundary Conditions	Type of Boundary Conditions	Velocity U	Pressure p	k, ω
Inlet	Type patch, faces	$U = U_{ship}$	$\partial p/\partial n = 0$	Specific value in Table 4
Outlet	Type patch, faces	$\partial U/\partial n = 0$	$\partial p/\partial n = 0$	$\partial k/\partial n = 0$; $\partial \omega/\partial n$
Top	Type patch, faces	$\partial U/\partial n = 0$	$p = p_\infty$	$\partial k/\partial n = 0$; $\partial \omega/\partial n$
Sides	Type patch, faces	$\partial U/\partial n = 0$	$\partial p/\partial n = 0$	$\partial k/\partial n = 0$; $\partial \omega/\partial n$
Bottom	Type patch, faces	$\partial U/\partial n = 0$	$p = p_\infty$	$\partial k/\partial n = 0$; $\partial \omega/\partial n$
Hull	No-slip condition	$U = 0$	$\partial p/\partial n = 0$	Wall function
Center plane	Symmetry Plane, faces	Symmetry		

For incompressible flows like the flow around a hull, the inlet boundary condition is usually located in front of the ship, where flow speed begins changing by the influence of the ship hull. Other boundary conditions such as the side, bottom, and top of the computational domain must also be specified as an input boundary to form the physical walls of the "numeric towing tank". This is the case where the flow is steadily moving around the fixed hull model and the flow boundaries (side, top, and bottom) parallel to the undisturbed flow can be specified as slip walls. For the flow with a free surface, the flow speed at the inlet boundary is set equal to the ship speed but in the opposite direction. The air speed is also set equal to the flow speed due to a no-wind condition is assumed. The outlet boundary condition is usually specified where the flow leaves the computational domain, and zero speed and pressure gradient conditions can be applied [23]. Referring to the method detailed in [25], the preliminary estimate and change the computational domain size in turn which are calculated according to the length between the perpendiculars (L_{PP}) of the ship model, then compute deviation (ΔR) between OpenFOAM-based total resistance value $(R_T)_{CFD}$ and model test value $(R_T)_{test}$ at design speed (8,5 knots for the M1317 boat and 7,5 knots for the M1319 boat) for each variation of the computational domain size to find the most suitable computational domain corresponding to the minimum deviation and nearest boundary positions.

Table 4. Resistance values and deviation at the case size of the computational domain [6]

Case size	Boundary positions of the computational domain					CFD-based resistance value R and deviation ΔR					
						M1317A			M1319		
	Inlet	Outlet	Sides	Top	Bottom	$(R_T)_{test}$ (N)	$(R_T)_{CFD}$ (N)	ΔR (%)	$(R_T)_{test}$ (N)	$(R_T)_{CFD}$ (N)	ΔR (%)
1	$1,5L_{pp}$	$5,0L_{pp}$	$2,5L_{pp}$	L_{pp}	L_{pp}	8977,8	10518,8	14,65	2826,6	3424,5	17,46
2	$2,0L_{pp}$	$5,0L_{pp}$	$2,5L_{pp}$	L_{pp}	L_{pp}		9201,4	2,43		2930,6	3,55
3	$2,5L_{pp}$	$5,0L_{pp}$	$2,5L_{pp}$	L_{pp}	L_{pp}		9199,5	2,41		2926,4	3,41
4	$1,5L_{pp}$	$4,0L_{pp}$	$2,0L_{pp}$	L_{pp}	L_{pp}		10510,2	14,58		3351,0	15,65
5	$2,0L_{pp}$	$4,0L_{pp}$	$2,0L_{pp}$	L_{pp}	L_{pp}		9201,4	2,43		2906,8	2,76
6	$2,5L_{pp}$	$4,0L_{pp}$	$2,0L_{pp}$	L_{pp}	L_{pp}		9202,3	2,44		2908,6	2,82
7	$2,0L_{pp}$	$3,0L_{pp}$	$1,5L_{pp}$	L_{pp}	L_{pp}		10397,0	13,65		3298,6	14,31

Based on the computed results shown in Table 4, it can be found the most suitable computational domain size for the study fishing boats is case 5 which is determined as described in Figure 5, where the bottom and top boundaries are located at $1L_{pp}$ from the free surface, while the inlet, outlet, and sides boundaries are located at $2L_{pp}$, $4L_{pp}$, and $2L_{pp}$ from the model hull, respectively. Also on this figure, the top right figure shows the flow field distribution, which exported from OpenFOAM software, is steadily, smoothly, and without occurring the wall-tank effect.

ISSN- 2394-5125 VOL 7, ISSUE 15, 2020

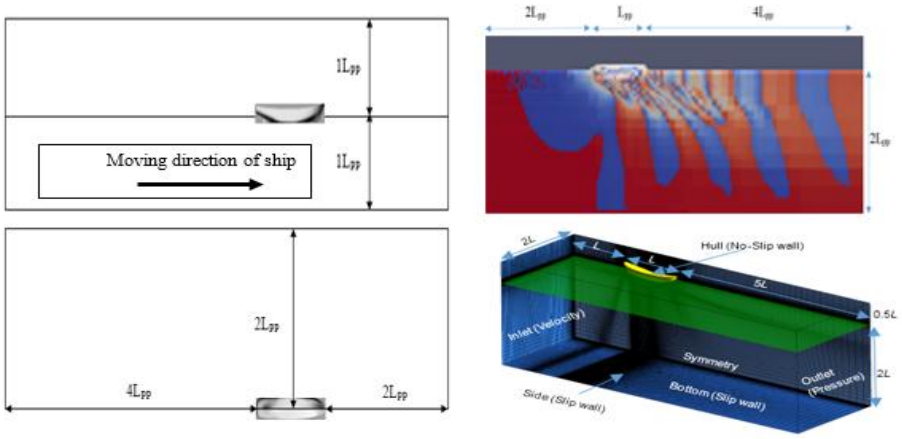

Figure 5. Computational domain and boundary condition

3. Turbulence model parameters

Since the flow around the ship hull is always turbulent, it is necessary to specify the values of the turbulence parameter at the inlet boundary of the computational domain to simulate this effect. The parameters of the SST k-ω turbulence model used in this study consist of the turbulent kinetic energy (k), specific rate dissipation (ω), and rate of dissipation turbulent kinetic energy (ε), which will be determined using the following empirical equations [18]:

$$k = \frac{3}{2}(IU)^2 \;;\; \varepsilon \square\square\square \frac{\sqrt{k}}{L_{PPm}} \;;\; \omega = 10\,\frac{U}{L_{PPm}} \tag{14}$$

where I is turbulent intensity; U is the speed of incoming flow at inlet boundary determined equal to the speed of the model U_M, m/s; L_{PPm} is the length between perpendiculars of the model, m.

Similar to the above method, estimating some values of turbulent intensity (I) within the empirical range (I is less than 0,01 for a low-speed, from 0,01 to 0,1 for medium-speed and greater than 0,1 for high-speed ship), and calculating the value of remaining parameters using formulas (14) [18]. Computing the deviation (ΔR) between the OpenFOAM-based total ship resistance value $(R_T)_{CFD}$ and the corresponding test value $(R_T)_{test}$ at different speeds of the computational boat models for each case of the determined turbulence model parameters to choose the most appropriate case corresponding to the deviation (ΔR) is the minimum as shown in Table 5 [6].

Table 5. The parameter values of SST k- ω turbulence model for fishing boat hulls

Quantities	Unit	M1317A Hull					M1319 Hull				
U_M	m/s	0,640	1,251	1,381	1,679	1,758	1,166	1,369	1,460	1,772	1,807
Fn		0,12	0,24	0,27	0,33	0,34	0,26	0,30	0,32	0,39	0,40
I		0,006	0,007	0,008	0,009	0,010	0,006	0,007	0,008	0,009	0,010
k		0,00002	0,0001	0,0002	0,0003	0,0005	0,0001	0,0001	0,0002	0,0004	0,0005
□		2,3581	4,6094	5,0884	6,1864	6,4775	5,5156	6,4759	6,9063	8,3822	8,5478
ε		0,0017	0,0040	0,0050	0,0068	0,0079	0,0041	0,0056	0,0068	0,0092	0,0105
$(R_T)_{CFD}$	N	689,3	3435,6	4476,3	9540,5	11907,9	1526,6	2472,6	2919,1	6658,4	7615,8
$(R_T)_{test}$	N	611,3	3135,3	4361,7	8988,1	10548,0	1360,5	2401,1	2826,6	6250,9	6969,2
ΔR (%)	%	11,31	8,74	2,56	5,79	11,42	10,88	2,89	3,17	6,12	8,49

From the results in Table 4, it can be seen the most suitable value of the turbulent intensity (I), which corresponds to the minimum deviation, equal to 0,008 for M1317A and 0,007 for M1319. The most suitable value of the turbulent intensity (I) for the two study boats differs slightly, probably due to the fuller hull form of the M1317A boat than that of the M1319 boat, which is in the ratio of the length to the breadth of the M1317A

ISSN- 2394-5125 VOL 7, ISSUE 15, 2020

boat is smaller than that of the M1319 boat, while the block coefficient value (C_b) of the M1317A boat is greater than that of the M1319 boat. In general, the SST k-ω turbulence model parameters can be determined by pre-selecting value of turbulent intensity (I) within range (0,007 – 0,008) to calculate the value of the parameters of the SST k-ω turbulence model consist of the turbulent kinetic energy (k), specific rate dissipation (ω), and rate of dissipation turbulent kinetic energy (ε) according to the empirical equations (14).

D. Computational results

The flow around the ship hulls is computed using the open-source code of incompressible multiphase solver that is included in OpenFOAM libraries (*InterFoam* and/or *LTSInterFoam*) []. This solver uses the finite volume approach and PIMPLE algorithm, which is combined the PISO and SIMPLE algorithms, to approximate the pressure and velocity field for transient problems. The theory of this solver can be found in [20], in which the principal of the algorithm is as follows. Within a one-time step, we will implement to search a steady-state solution with under-relaxation. After finding a solution, we will move on to the next time step, and for these, we need to use the so-called outer correction loops, to ensure that *explicit* parts of the equations are converged [1]. When a solution reaches a tolerance criterion which is defined in the steady-state calculation, leave the outer correction loop, and move on time. The advantage of the PIMPLE algorithm is that it is possible to use a larger Courant number (C_R<<1), so the time step can be greatly increased [20] For computing the free surface of the flow around the hull, the known hydrostatic pressure field distributed according to the relative positions of the undisturbed free surface must also be specified at the outlet boundary. Running the OpenFOAM solver to predict the resistance of the computational fishing boats obtained some results as follows:

1. Hydrodynamic Forces

Figure 6 shows the fluctuation of the hydrodynamic forces occurring at two values of the ship speed or Froude number of two computation fishing boat models where the values of the viscous and pressure force in the x-axis direction are plotted for each time step of the computation process. The convergence rate of the CFD resistance solution is quite fast with about 4000 iteration steps. Similar results are also obtained for other values of speed or Froude number (Fn) within the operating speed range of these fishing boats (see reference [6]). This allows us to conclude that the solution method and value of the initial parameters selected in this study are appropriate to Vietnamese fishing boats due to the accuracy and reliability of the CFD-based resistance value.

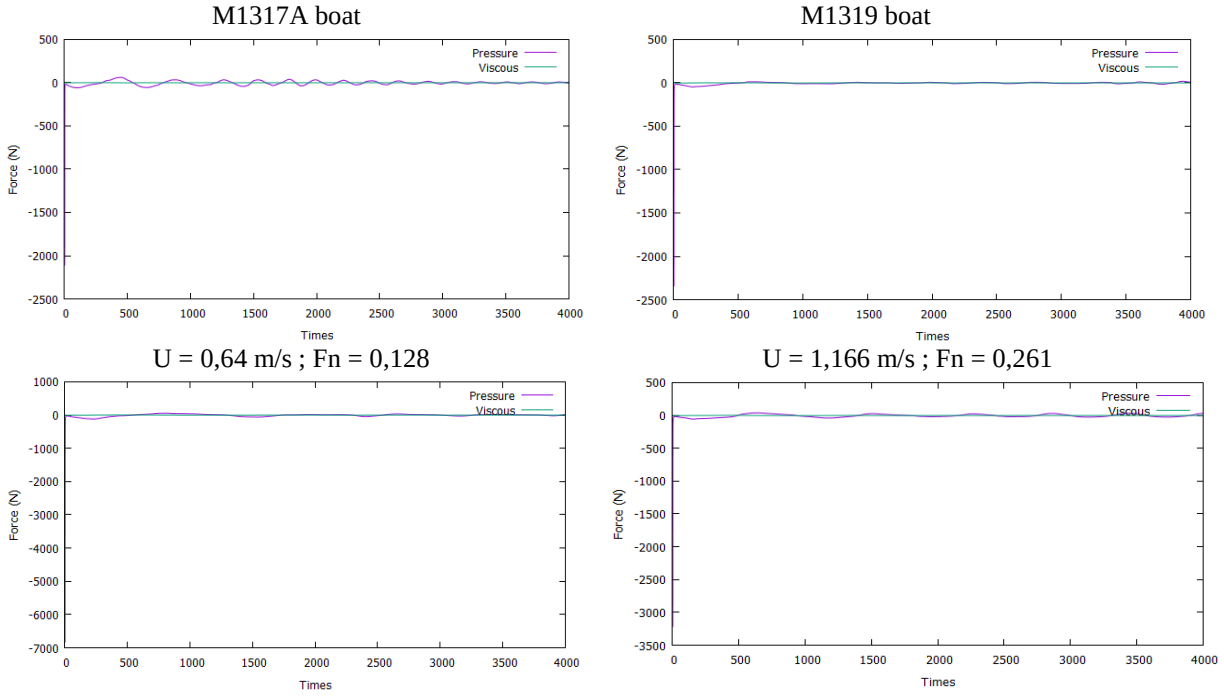

Figure 6. The hydrodynamic forces for iteration

2. Total resistance and its components

Table 6 and Figure 7 present the values and curves of the total resistance and its components which are

ISSN- 2394-5125 VOL 7, ISSUE 15, 2020

computed based on CFD with the initial parameters determined for two study hulls [6]. Also in this table and figure, a comparison between CFD-base total resistance values and curves with the model test data shown the relative deviation in all computation cases is less than 3%. Since the resistance is computed for different speed at the inlet in the same mesh typology and size so the deviations for each case is reasonable

Table 6. The values of the total and component resistance of two computation boats

Properties	Notation	Unit	M1317A boat					M1319 boat				
Model speed	U_M	m/s	0.640	1,251	1,381	1,679	1,758	1,166	1,369	1,46	1,772	1,807
Ship speed	U_S	m/s	1,69	3,31	3,65	4,44	4,65	3,08	3,62	3,86	4,69	4,78
		Knots	3,3	6,4	7,1	8,6	9,0	6,0	7,0	7,5	9,1	9,3
Model wetted area	Ω_M	m^2	1,919	1,919	1,919	1,919	1,919	0,92	0,92	0,92	0,92	0,92
Ship wetted area	Ω_S	m^2	94,02	94,02	94,02	94,02	94,02	45,08	45,08	45,08	45,08	45,08
Froude number	Fn	-	0,126	0,245	0,271	0,329	0,345	0,261	0,312	0,326	0,396	0,404
Model pressure resistance, CFD	$(R_{PM})_{CFD}$	N	0,722	5,409	8,588	21,103	24,02	1,628	3,853	4,554	13,64	15,74
Model viscous resistance, CFD	$(R_{VM})_{CFD}$	N	1,027	3,888	4,462	5,764	6,527	2,257	3,301	3,744	4,883	4,895
Ship pressure resistance coefficient	C_P	-	0,002	0,004	0,005	0,008	0,008	0,003	0,004	0,005	0,009	0,01
Ship viscous resistance coefficient	C_V	-	0,003	0,003	0,002	0,002	0,002	0,004	0,004	0,004	0,003	0,003
CFD-based ship pressure resistance	$(R_P)_{CFD}$	N	247,5	1855,2	2945,7	7238,2	8544,5	558,5	1321,7	1562,1	4679,8	5398,8
CFD-based ship viscous resistance	$(R_V)_{CFD}$	N	352,1	1333,5	1530,6	1977,0	2238,8	558,5	1132,4	1284,3	1675,0	1679,0
CFD-based ship total resistance	$(R_T)_{CFD}$	N	599,6	3188,7	4476,3	9215,2	10783,3	1332,8	2454,1	2846,4	6354,8	7077,8
Total ship resistance (test)	$(R_T)_{test}$	N	611,3	3135,3	4361,7	8988,1	10548	1360,5	2401,1	2826,6	6250,9	6969,2
Deviation	ΔR	%	-1,91	1,70	2,63	2,53	2,23	-2,04	2,21	0,70	1,66	1,56

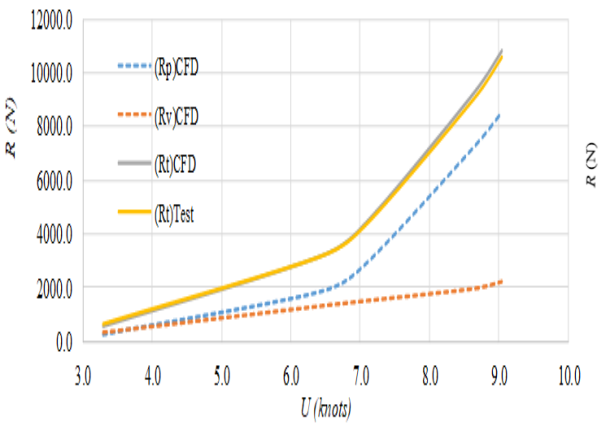

(a) M1317 boat

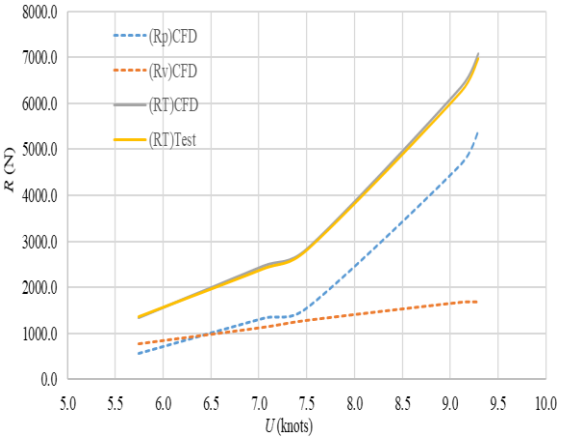

(b) M1319 boat

ISSN- 2394-5125 VOL 7, ISSUE 15, 2020

Figure 7. Resistance curves of M1317A and M1319 fishing boats

From those results, some comments can be drawn as follows:

(a) Viscous resistance, R_V

The value of the viscous resistance or frictional resistance increases linearly with the ship speed. It is perfectly suited to the test that force is proportional to the wetted area and speed of the hull. In this method, the frictional resistance is a component of the resistance which is obtained directly by integrating the shear stresses over the wetted area of the hull in the direction of ship motion. For a Newtonian fluid, the shear stress on the hull surface will be proportional to the ship speed, $\tau = \mu(\partial U/\partial y)_{wall}$, so when compared with theory, the tendency of the viscous resistance curve which is obtained based on computation above is perfectly reasonable.

(b) Pressure resistance, R_P

The pressure resistance, in this study, is determined by integrating the normal force acting on the hull with the effect of a free surface. Such force is dominated by the effect of the waves caused by moving of the ship in calm water, so pressure resistance is also named wave-making resistance The OpenFOAM-based pressure resistance component curve of the computational boats as presented in Figure 7, changes with the same trend as other studies in ship resistance prediction. Specifically, in the low-speed range, this resistance component increases slowly compared to the viscous resistance component, and in the medium and high-speed range, it increases significantly. As ship speed increases from low to medium range, the slope of the pressure resistance curve increases proportionally, as it continues to increase to high range and reaches an ultimate value, a small change in speed can result in a significant change in the pressure resistance component. It increases sharply and reaches the ultimate value, as follows:

- For M1317 fishing boat (Figure 7a)

Within the speed range (3,3 ÷ 6,8) knots, the pressure resistance value of the M1317 boat tends to increase moderately. And within the speed range (6,8 ÷ 9,0) knots, the slope of the pressure resistance curve of this boat tends to increase rapidly. It means that within a high-speed range, pressure resistance is dominant and its change greatly affects the total resistance of this hull. It can be seen at a speed of 9,0 knots, the pressure resistance occupies about 79% of the total resistance, and is perfectly consistent with the known theory and practice of ship resistance. Also from the existing total resistance curve, an ultimate ship speed value has not been seen, probably because the computed speed range is not large enough so this point has not appeared. However, the optimal speed under the current load condition of the M1317A fishing boat is recommended at about 7.0 knots.

- For M1319 fishing boat (Figure 7b)

The pressure resistance curve of the M1319 boat has an advantage over the M1317A boat. Specifically, the slope of the pressure resistance curve of the M1319 boat within the speed range (7,0 ÷ 7,5) knots is almost zero, proving that this boat operates most effectively within this speed range, thus the design speed of this boat should be chosen within this speed range. It can also be seen that when the ship speed exceeds 9,1 knots, the slope of the pressure resistance curve increases rapidly, proving this speed is the ultimate value of the M1319 hull. Therefore, under the current load condition, the design speed of the M1319 should not be greater than this ultimate value. Similar to the pressure resistance curve of the M1317A above, the change of pressure resistance curve of the M1319 also influences the change in the total resistance curve of this boat.

(c) Total resistance, R_T

The change of the total resistance curves of both computational boats is mainly influenced by the pressure resistance curves, so these curves have also the features similar to the pressure resistance curves, as follow:

- The optimal operating speed of both study boats in terms of resistance is the same and approximates to 7,5 knots. If the design speed of the computational boats is greater than this value, the pressure resistance will increases significantly, resulting in a rapid increase in the total resistance, even if it has not reached the maximum speed.

- The pressure resistance proportion of both study boats, if considered within the speed range less than the ultimate speed, occupies a relatively large proportion of the total resistance. Specifically, the pressure resistance value approximate to 79% at Fn = 0,345 for the M1317A boat, and approximate to 73% at Fn = 0,396 for the M1319 boat of their total resistance value. Although the fishing boats are classified as a low Froude number, it is probably quite different from the typical merchant ship.

ISSN- 2394-5125 VOL 7, ISSUE 15, 2020

- On the total resistance curves of both study boats, there exists a value of ultimate speed, where the total resistance value of both boats begins to increase suddenly. This ultimate value approximates to 9,0 knots for the M1317A boat and approximates to 9,1 knots for the M1319 boat. These results show that the total resistance curve of the M1317A boat has many advantages compared to the M1319 boat. Specifically, the curvature of the resistance curves of the M1317A boat does not increase suddenly, so the ultimate speed of the M1317A boat might be higher than that of the M1319 boat.

3. Flow field feature

Figure 8 shows the numerical simulation results of the flow field around two computation boats, including the contours of the volume fraction of water and air, turbulent kinetic energy (k), the distribution of pressure and speed, and the wave pattern at symmetry and free surface plane. These are obtained at Froude number of 0,326 correspondings to a speed of 1,67 m/s for the M1317A model, and at Froude number of 0,336 correspondings to a speed of 1,77 m/s for the M1319 model. An explanation of the features and physical significance for the sub-figures in this figure can be presented as follows:

- Figure 8a presents the computation result of the volume fraction, where the volume fraction of water equals one, while the volume fraction of air equals zero for both study boat models. This result shows that the equation of volume fraction was successfully computed using the VOF method.

- Figure 8b shows that the values of the turbulent kinetic energy (k) fluctuate significantly in the bow and stern region within the flow around two the study boat hulls due to the effects of the free surface, and the sudden changes of pressure and speed gradient in these regions. It is reasonable that the wave-making resistance dominates under the current operating condition of both computational fishing boats.

- Figure 8c shows the contours of the pressure distribution in the flow around two hulls are plotted at the symmetry planes. As can be seen, two above pressure fields are a similar trend. Using the suitable code in OpenFOAM, it can be seen that the high-pressure areas at the bow and stern region, where higher pressure values can be found in the stagnant area at the bow. It can be seen that the pressure gradient in the stagnant area within the bow and stern region will be decreased until they reach the lowest values as can be seen in the previous figure.

- The pressure will be increased again within the stern region due to the effect of stern geometry on the distribution of the speed field in the flow around the computational hulls. Downstream of this position, the pressure will decrease again and extends approximately over the entire mid-hull part as the hull cross-sections are nearly unchanged in this region. These results are entirely consistent with theory and practice. In addition, the effects of the bow and stern waves on pressure distribution around the hulls are detected at the free surface. This figure also shown a wave profile on the hull with wavelength equals half the hull length. As mentioned above, the pressure resistance component occupies a large proportion of the total resistance, approximates to 79% at Froude number of 0,345 for M1317A fishing boat, and approximates to 73% at Froude number of 0,396 for M13179 boat as shown in Table 3. Such type of resistance component mainly maintains the wave system around the ship hull. Therefore, the information on wave patterns plays an important role when improving the hull form to reduce the wave-making.

- Figure 8d shows the form of the wave pattern contours which are captured using this method. The ship wave system in the wake contains the divergence and transverse wave systems [2]. The result shows that the entrance angle of the bow wave approximates to (35 - 46) degrees, and the wavelength on the ship hulls equals half of the length of the ship design waterline. Those values are quite larger comparing to the merchant ships.

IV. CONCLUSIONS

Based on the obtained research results, the specific conclusions can be drawn as follows:

- The turbulent flow around two study hulls has been simulated using the OpenFOAM code. The total resistance values of two computational fishing boats have been compared well with their available model test results at five values of the Froude number (see Table 6).

- The technique of generation 3D hull geometry in *.STL file format using OpenFOAM code matches perfectly the 3D hull surface model which is exported by popular CAD software. It not only ensures the reliability and accuracy of the computational boat resistance results but also reduces the consuming-time to generate the computational mesh in post-processing. It also enables us to code for generating the mesh automatically from the 3D hull geometry.

ISSN- 2394-5125 VOL 7, ISSUE 15, 2020

- The approach to use OpenFOAM open-source with RANSE and SST k-ω turbulence model, as well as VOF method and PIMPLE algorithm, is accurate and applicable to predict the resistance of fishing boats, which have a small size, low speed, and low-Re turbulence flow regime like Vietnamese wooden fishing boat type.

- The setting and determining the suitable values for the input parameters of the CFD solver, including the computational domain size, the position and value of the boundary conditions, and turbulence model parameters greatly affect the accuracy and reliability of the final result. Also in this paper, the suitable values of the computational domain size (see Figure 5), the position and value of the initial boundary conditions (see Table 3), and the turbulence model parameters (see Table 5) were published. It is the basis for accurate and reliable prediction and analysis of the resistance components of small and low-speed wooden fishing boats. They are quite different from published data for conventional cargo and military ships [3].

- In the preliminary design of fishing boats in particular and Vietnamese wooden fishing boats in general, the design speed under usual loading conditions should be within (7,5 – 8,5) knots because outside this range, the boats may not operate well in terms of hydrodynamics.

- These research results are the basic for solving many different important problems in ship design, especialy the optimization problem of the wooden fishing boat hulls.

M1317A boat M1319 boat

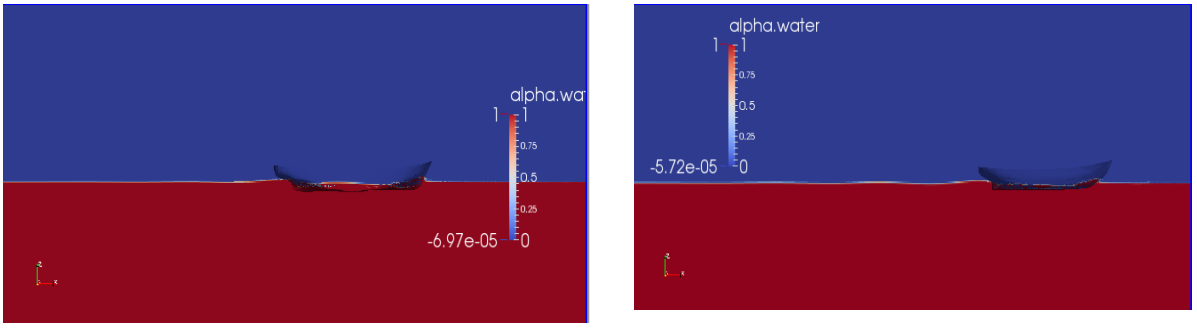

(a) The volume fraction of water at the symmetry plane

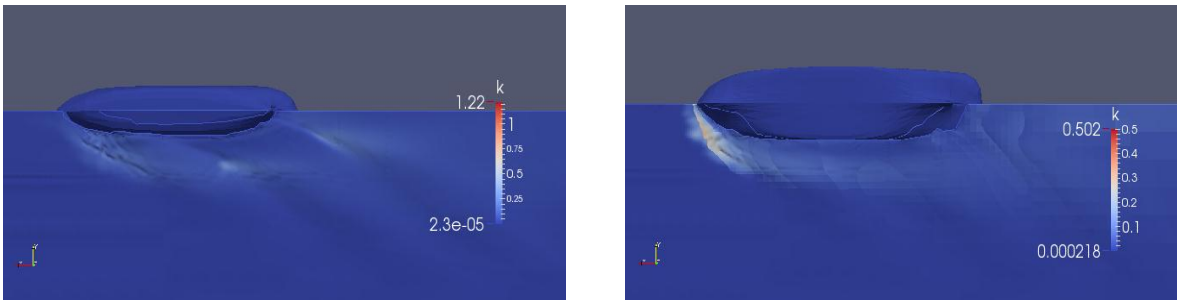

(b) Turbulent kinetic energy contours at a free surface

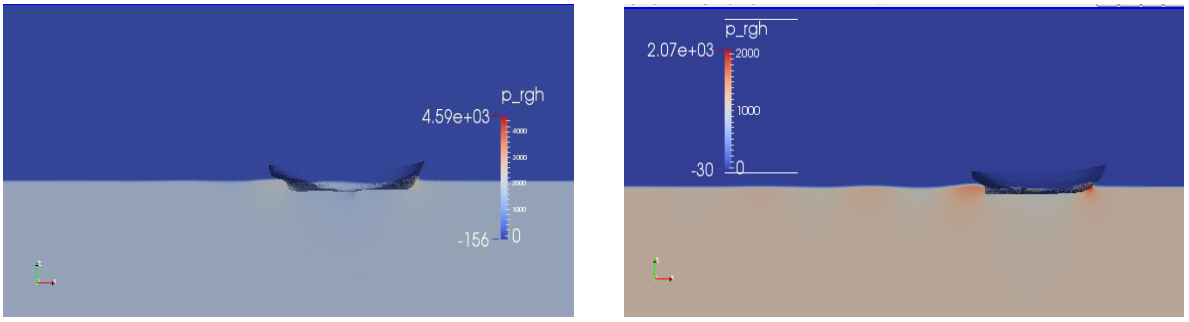

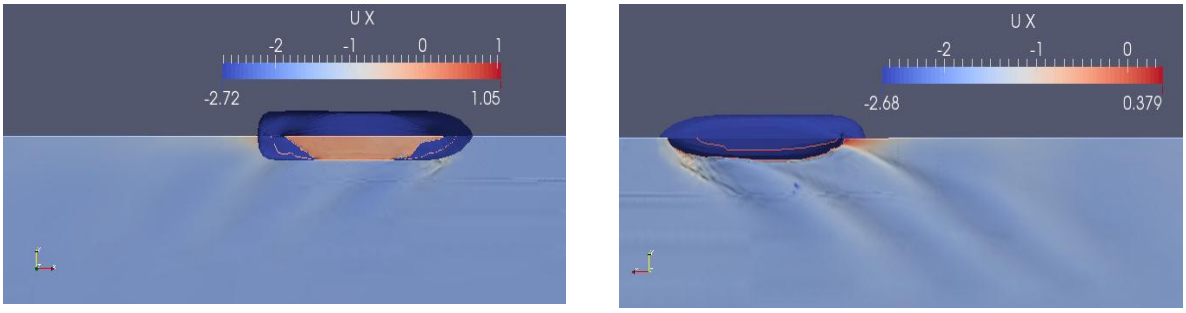

(c) Pressure and speed distribution contour at symmetry plan and on the free surface

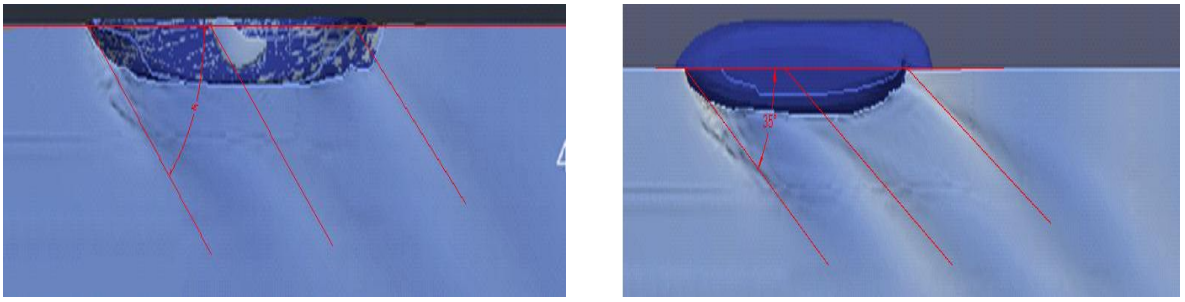

(d) Wave patterns contour

Figure 8. The numerical simulation result of the flow around two study boat hulls

V. REFERENCES

[1] John F. Wendt. (2009). "Computational Fluid Dynamics". *An Introduction. Springer.*

[2] Beltram.V (2000)."Practical Ship Hydrodynamics", *Oxford, MA, Butter worth Heinemann.*

[3] Larsson.L, Stern. F and Visonneau. M. (2011). "CFD in ship hydrodynamics", *Results of the Gothenburg 2010 workshop in MARINE 2011, IV International Conference on Computational Methods in Marine Engineering, MARINE 2011.*

[4] Raven H. C, Van der Ploeg A., Starke A. and Ecal. (2008). "Towards a CFD-based prediction of ship performance - progress in predicting full-scale resistance and scale effects". *Proceedings of RINA-CFD, London, UK.*

[5] Petros Voxakis. (2012). "Ship hull resistance calculation using CFD methods". *Massachusetts Institute of Technology.*

[6] Toan Le Van, Thai Gia Tran (supervisor). (2017). "Application of CFD to predict the resistance of Vietnamese wooden fishing boats. Nha Trang Univeristy", *Doctoral Thesis.*

[7] Ebrahimi A.(2010). "Numerical Study on Resistance of a Bulk Carrier Vessel Using CFD Method". *Journal of the Persian Gulf, Vol.3, No.10, 1-6.*

[8] Gaggero S., Villa. D, Ferrado. M. (2014). "An open source approach for prediction of planning hull resistance", *10th Symposium on High Speed Marine Vehicles. HSMV2014, At Naples, Italy.*

[9] Ozdemir, Yavuz Hakan, Dogrul, Ali, Barlas, Boris, Cosgun, Taner. (2016)."A Numerical Application to Predict the Resistance and Wave Pattern of Kriso Container Ship*", Brodogradnja. Vol .67, No2, 47-65.*

[10] Salina Aktar, Goutam Kumar Saha, Md. Abdul Alim. (2013). "Numerical computation of wave resistance around Wigely hull using computational fluid dynamics tools", *Advance Shipping and Ocean Engineering. Vol. 2, No 3, 84-95.*

[11] ITTC. (2011). "Practical Guidelines for Ship CFD Applications". *ITTC - Recommended Procedures and Guidelines.*

[12] Jacquin E., Derbanne Q., Bellevre D., Cordier S. (2004), *Hull form optimization using a free surface RANSE solver,* 25th Symposium on Naval Hydrodynamics.

[13] Park S. H., Park S. W., Rhee S. H., Lee S. B., Choi J. E., Kang S. H. (2012). "CFD code development for the prediction of the ship resistance using open source libraries". *Journal of computational fluids engineering, 17(2), 21-27 (in Korean).*

[14] Maki K. (2011). "Ship resistance simulations with OpenFOAM", *In 6th OpenFOAM Workshop.*

[15] Justus Heimann. (2013). "CFD Based Optimization of the Wave-Making Characteristics of Ship Hulls". *Technischen Universität Berlin (Doctoral Thesis).*

ISSN- 2394-5125 VOL 7, ISSUE 15, 2020

[16] Wilcox D. C. (1988). Assessment of the scale-determining equation for advanced turbulence models", AlAA Journal. Vo1.26,1299-1310.
[17] Menter F. R. (1993). "Zonal two equation k-ω turbulence models for aerodynamic flows". *AIAA Paper 93-2906.*
[18] Menter F. R (1994). "Two-Equation Eddy-Viscosity Turbulence Models for Engineering Applications", *AIAA Journal, Vol. 32, No 8. pp. 1598-1605.*
[19] Hanjalic K., Launder B.E. (1972). "A Reynolds stress model of turbulence and its application to thin shear flows". *J. Fluid Mech, Vol. 52, No. 2, 609-638.*
[20] (2014). "The OpenFOAM foundation". *Programmer's Guide.*
[21] Hirt C. W. and Nichols B. D. (1981). "Volume of Fluid (VOF) method for the dynamics of free boundaries". *Journal of Computational Physics, Vol. 39, No.1, 201-225.*
[22] Katuri Samarpana, Ajay konapala, Duvvada Ramesh. (2013). "Computational investigation of free surface flow around a ship hull". *International Journal of Application or Innovation in Engineering & Management (IJAIEM). Vol. 2 No 5.*
[23] Pranzitelli A., Nicola C., Miranda S. (2011). "Steady-state calculations of free surface flow around ship hulls and resistance predictions", *High Speed Marine Vehicles (IX HSMV), Naples, Italy.*
[24] Thai Gia Tran. (2020). Improving the accuracy of ship resistance prediction using computational fluid dynamics tool. *International Journal on Advance Science Engineering Information Technology.*